simulations consisted of an initial minimization of water molecules followed by 100 ps of MD with the protein restrained. Following positional restraints MD, all restraints on the protein were removed and MD continued for a further 50 ns. Coordinates were archived throughout the simulation at 100 ps intervals.

Cell culture and plasmid transfection. HaCaT immortalized keratinocytes and HeLa cells were maintained in Dulbecco's modified Eagle's medium (GIBCO, Grand Island, NY, USA) supplemented with 10% (v/v) fetal bovine serum. Normal human epidermal keratinocytes (NHEK) from neonatal foreskin (NHEK; Lonza, Allendale, NJ, USA) were cultured in keratinocyte growth medium (KGM; Lonza). Three different transfections (K14WT, K14A413P and K14A413T) into HaCaT cells or HeLa cells (2 μg of plasmid in 6-well dishes) were performed using Lipofectamine LTX (Invitrogen) according to the manufacturer's instructions. Three different plasmids (K14WT, K14A413P and K14A413T) were transfected respectively into NHEK (5 μg of plasmid in 6-well dishes) with electroporation using Amaxa Nucleofector apparatus (Amaxa, Cologne, Germany). Also, three different transfections into HaCaT cells, including K14A413P alone (2 μg of plasmid in 6-well dishes), a combination of equal amounts of K14A413P (1 μg) and K14WT (1 μg) (K14A413P/K14WT), and a combination of equal

amounts of K14A413P (1 μg) and K14A413T (1 μg) (K14A413P/K14A413T) were performed using Lipofectamine LTX (Invitrogen).

Immunoblot analysis. At 24 h after transfection, HaCaT cells were lysed in Laemmli buffer (consisting of 62.5 mM Tris-HCl (pH 6.8), 3% SDS, 5% mercaptoethanol) on ice for 10 min, cell debris was removed by centrifugation at 14,000 rpm for 5 min, and supernatant was collected. Supernatants were electrophoresed on a NuPAGE 4–12% bis-Tris gel (Invitrogen) and transferred to a PVDF membrane. The membrane was incubated with horseradish peroxidase (HRP) conjugated anti-V5 antibody (Invitrogen) for one hour at room temperature, and the blots were detected using the ECL Plus Detection Kit (GE Healthcare).

Confocal laser analysis. At 24 h after transfection, the cells were washed with phosphate-buffered saline and fixed with methanol. A FITC-conjugated anti-V5 antibody (Invitrogen) was used to detect transfected cells. All cells were observed using a confocal laser scanning microscope (Olympus Fluoview FV300). The cells with keratin aggregates were counted in five different areas, two from each experimental replicate (a mean of 42 cells from each replicate) as described previously (Yasukawa *et*

al., 2002), and the results obtained from the ten counts were expressed as the mean ± SEM.

Ethics. The medical ethics committee of Hokkaido University Graduate School of Medicine approved all studies. The study was conducted according to the Declaration of Helsinki Principles. Participants or their legal guardians gave written informed consent.

ACKNOWLEDGEMENTS

We thank Ms. Yuko Hayakawa for her technical assistance. This work was supported by Health and Labor Sciences Research grants from the Ministry of Health, Labor, and Welfare of Japan (to H.S.) for Research on Measures for Intractable Diseases. BJS gratefully acknowledges infrastructure support from the NHMRC IRIISS grant #361646 and a Victorian State Government OIS grant.

References

Albers K, Fuchs E (1987) The expression of mutant epidermal keratin cDNAs transfected in simple epithelial and squamous cell carcinoma lines. *J Cell Biol* 105:791-806.

Boukamp P, Petrussevska RT, Breitkreutz D, Hornung J, Markham A, Fusenig NE (1988) Normal keratinization in a spontaneously immortalized aneuploid human keratinocyte cell line. *J Cell Biol* 106:761-771.

Bussi G, Donadio D, Parrinello M (2007) Canonical sampling through velocity rescaling. *J Chem Phys* 126:014101.

Chao SC, Yang MH, Lee SF (2002) Novel KRT14 mutation in a Taiwanese patient with epidermolysis bullosa simplex (Kobner type). *J Formos Med Assoc* 101:287-290.

Conway JF, Parry DAD (1990) Structural features in the heptad substructure and longer range repeats of two-stranded alpha-fibrous proteins. *Int J Biol Macromol* 12:328-334.

Coulombe PA, Fuchs E (1990) Elucidating the early stages of keratin filament assembly. *J Cell Biol* 111:153-169.

Coulombe PA, Hutton ME, Letai A, Hebert A, Paller AS, Fuchs E (1991) Point mutations in human keratin 14 genes of epidermolysis bullosa simplex patients: genetic and functional analyses. *Cell* 66:1301-1311.

Coulombe PA, Kerns ML, Fuchs E (2009) Epidermolysis bullosa simplex: a paradigm for disorders of tissue fragility. *J Clin Invest* 119:1784-1793.

Cummins RE, Klingberg S, Wesley J, Rogers M, Zhao Y, Murrell DF (2001) Keratin 14 point mutations at codon 119 of helix 1A resulting in different epidermolysis bullosa simplex phenotypes. *J Invest Dermatol* 117:1103-1107.

Essman U, Perela L, Berkowitz ML, Darden T, Lee H, Pedersen LG (1995) A smooth particle mesh Ewald method. *J Chem Phys* 103:8577-8592.

Fine JD, Eady RA, Bauer EA, Bauer JW, Bruckner-Tuderman L, Heagerty A, *et al.* (2008)

The classification of inherited epidermolysis bullosa (EB): Report of the Third International Consensus Meeting on Diagnosis and Classification of EB. *J Am Acad Dermatol* 58:931-950.

Fiser A, Sali A (2003) Modeller: generation and refinement of homology-based protein structure models. *Methods Enzymol* 374:461-491.

Groves RW, Liu L, Dopping-Hepenstal PJ, Markus HS, Lovell PA, Ozoemena L, *et al.* (2010) A homozygous nonsense mutation within the dystonin gene coding for the coiled-coil domain of the epithelial isoform of BPAG1 underlies a new subtype of autosomal recessive epidermolysis bullosa simplex. *J Invest Dermatol* 130:1551-1557.

Hattori N, Komine M, Kaneko T, Shimazu K, Tsunemi Y, Koizumi M, *et al.* (2006) A case of epidermolysis bullosa simplex with a newly found missense mutation and polymorphism in the highly conserved helix termination motif among type I keratins, which was previously reported as a pathogenic missense mutation. *Br J Dermatol* 155:1062-1063.

Hatzfeld M, Franke WW (1985) Pair formation and promiscuity of cytokeratins: formation in vitro of heterotypic complexes and intermediate-sized filaments by homologous and heterologous recombinations of purified polypeptides. *J Cell Biol* 101:1826-1841.

Hatzfeld M, Weber K (1990) The coiled coil of in vitro assembled keratin filaments is a heterodimer of type I and II keratins: use of site-specific mutagenesis and recombinant protein expression. *J Cell Biol* 110:1199-1210.

Henikoff S, Henikoff JG (1992) Amino acid substitution matrices from protein blocks. *Proc Natl Acad Sci U S A* 89:10915-10919.

Herrmann H, Strelkov SV, Feja B, Rogers KR, Brettel M, Lustig A, *et al.* (2000) The intermediate filament protein consensus motif of helix 2B: its atomic structure and contribution to assembly. *J Mol Biol* 298:817-832.

Hess B (2008) P-LINCS: A Parallel Linear Constraint Solver for molecular simulation. *J Chem Theory Comput* 4:116-122.

Hess B, Kutzner C, van der Spoel D, Lindahl E (2008) GROMACS 4: Algorithms for Highly Efficient, Load-Balanced, and Scalable Molecular Simulation. *J Chem Theory Comput*

4:435-447.

Hut PH, v d Vlies P, Jonkman MF, Verlind E, Shimizu H, Buys CH, *et al.* (2000) Exempting homologous pseudogene sequences from polymerase chain reaction amplification allows genomic keratin 14 hotspot mutation analysis. *J Invest Dermatol* 114:616-619.

Jorgensen WL, Tirado-Rives J (1988) The OPLS potential functions for proteins. Energy minimizations for crystals of cyclic peptides of crambin. *J Am Chem Soc* 110:1657-1666.

Lane EB, Rugg EL, Navsaria H, Leigh IM, Heagerty AH, Ishida-Yamamoto A, *et al.* (1992) A mutation in the conserved helix termination peptide of keratin 5 in hereditary skin blistering. *Nature* 356:244-246.

Letai A, Coulombe PA, Fuchs E (1992) Do the ends justify the mean? Proline mutations at the ends of the keratin coiled-coil rod segment are more disruptive than internal mutations. *J Cell Biol* 116:1181-1195.

Li SC, Goto NK, Williams KA, Deber CM (1996) Alpha-helical, but not beta-sheet, propensity of proline is determined by peptide environment. *Proc Natl Acad Sci U S A* 93:6676-6681.

Linard B, Bezieau S, Benlalam H, Labarriere N, Guilloux Y, Diez E, *et al.* (2002) A ras-mutated peptide targeted by CTL infiltrating a human melanoma lesion. *J Immunol* 168:4802-4808.

MacArthur MW, Thornton JM (1991) Influence of proline residues on protein conformation. *J Mol Biol* 218:397-412.

Moll R, Franke WW, Schiller DL, Geiger B, Krepler R (1982) The catalog of human cytokeratins: patterns of expression in normal epithelia, tumors and cultured cells. *Cell* 31:11-24.

Nelson WG, Sun TT (1983) The 50- and 58-kdalton keratin classes as molecular markers for stratified squamous epithelia: cell culture studies. *J Cell Biol* 97:244-251.

Sapio MR, Posca D, Troncone G, Pettinato G, Palombini L, Rossi G, *et al.* (2006) Detection of

BRAF mutation in thyroid papillary carcinomas by mutant allele-specific PCR amplification (MASA). *Eur J Endocrinol* 154:341-348.

Schweizer J, Bowden PE, Coulombe PA, Langbein L, Lane EB, Magin TM, *et al.* (2006) New consensus nomenclature for mammalian keratins. *J Cell Biol* 174:169-174.

Smith TA, Steinert PM, Parry DAD (2004) Modeling effects of mutations in coiled-coil structures: case study using epidermolysis bullosa simplex mutations in segment 1a of K5/K14 intermediate filaments. *Proteins* 55:1043-1052.

Sorensen CB, Andresen BS, Jensen UB, Jensen TG, Jensen PK, Gregersen N, *et al.* (2003) Functional testing of keratin 14 mutant proteins associated with the three major subtypes of epidermolysis bullosa simplex. *Exp Dermatol* 12:472-479.

Steinert PM (1990) The two-chain coiled-coil molecule of native epidermal keratin intermediate filaments is a type I-type II heterodimer. *J Biol Chem* 265:8766-8774.

Steinert PM, Marekov LN, Parry DAD (1993) Conservation of the structure of keratin intermediate filaments: molecular mechanism by which different keratin molecules integrate into preexisting keratin intermediate filaments during differentiation. *Biochemistry* 32:10046-10056.

Stephens K, Ehrlich P, Weaver M, Le R, Spencer A, Sybert VP (1997) Primers for exon-specific amplification of the KRT5 gene: identification of novel and recurrent mutations in epidermolysis bullosa simplex patients. *J Invest Dermatol* 108:349-353.

Strelkov SV, Herrmann H, Geisler N, Wedig T, Zimbelmann R, Aebi U, *et al.* (2002) Conserved segments 1A and 2B of the intermediate filament dimer: their atomic structures and role in filament assembly. *EMBO J* 21:1255-1266.

Strelkov SV, Schumacher J, Burkhard P, Aebi U, Herrmann H (2004) Crystal structure of the human lamin A coil 2B dimer: implications for the head-to-tail association of nuclear lamins. *J Mol Biol* 343:1067-1080.

Szeverenyi I, Cassidy AJ, Chung CW, Lee BT, Common JE, Ogg SC, *et al.* (2008) The Human Intermediate Filament Database: comprehensive information on a gene family involved in

many human diseases. *Hum Mutat* 29:351-360.

Thusberg J, Vihinen M (2009) Pathogenic or not? And if so, then how? Studying the effects of missense mutations using bioinformatics methods. *Hum Mutat* 30:703-714.

Yasukawa K, Sawamura D, Goto M, Nakamura H, Jung SY, Kim SC, *et al.* (2006) Epidermolysis bullosa simplex in Japanese and Korean patients: genetic studies in 19 cases. *Br J Dermatol* 155:313-317.

Yasukawa K, Sawamura D, McMillan JR, Nakamura H, Shimizu H (2002) Dominant and recessive compound heterozygous mutations in epidermolysis bullosa simplex demonstrate the role of the stutter region in keratin intermediate filament assembly. *J Biol Chem* 277:23670-23674.

Yoneda K, Furukawa T, Zheng YJ, Momoi T, Izawa I, Inagaki M, *et al.* (2004) An autocrine/paracrine loop linking keratin 14 aggregates to tumor necrosis factor alpha-mediated cytotoxicity in a keratinocyte model of epidermolysis bullosa simplex. *J Biol Chem* 279:7296-7303.

Figure legends

Figure 1. Clinical and ultrastructural features of a family with epidermolysis bullosa simplex

(a) Blisters and erosions are seen in the proband's right sole (arrows). (b) Toenail deformities are observed in the proband. (c) Ultrastructural features of the proband lesional skin sample show basal cell cytolysis (bar: 5 μm). No apparent keratin clumps are seen. (d) Pedigree of the proband's family. Affected individuals are indicated by black fill. The proband is indicated by an arrow.

Figure 2. *KRT14* mutation analysis

(a) The proband (III-2) is heterozygous for c.1237G>C (p.Ala413Pro) in *KRT14* (an arrow). (b) 2 out of 100 normal controls are heterozygous for c.1237G>A (p.Ala413Thr) (an arrow). (c) 1 out of 100 normal controls is homozygous for c.1237G>A (p.Ala413Thr) (an arrow). (d) The proband's uncle (II-3) is compound heterozygous for c.1237G>C (p.Ala413Pro) and c.1237G>A (p.Ala413Thr) (an arrow). (e) The wild-type sequence. (f) Mutant-allele specific amplification shows that affected family members (**Fig. 1d**) harbor c.1237G>C (p.Ala413Pro).

Figure 3. Molecular dynamics of the keratin heterodimer

(a) Sequences of the keratin helix motif and the heptad repeat positions in K5 and K14. (b-d) Molecular dynamics simulations. The changes in secondary structure due to an amino acid substitution were visualized through the molecular dynamics. These simulations were each run for 50.0 ns. Blue indicates the alpha-helix. The native (b) and p.Ala413Thr (c) peptides retain alpha-helix geometry (blue-colored) throughout the simulation. In contrast, increased instability in the alpha-helix was observed in the p.Ala413Pro mutant peptide (d) bound with K5, which is indicated by the appearance of yellow-colored turn motif (arrow heads). In the p.Ala413Pro peptide (d), the helical geometry at the C-terminus of both K14 and K5 is substantially compromised throughout the simulation - K5 is unstructured (coil geometry), and K14 alternates between coil, bend and turn geometries. (e) A schematic diagram of K14 structure. Note that Ala^{413} is located at the helix termination motif (HTM) of the keratin molecule. Ala^{413} corresponds to position 'b' of the heptad repeat (abcdefg), and is conserved among keratin polypeptides. (f) K14 amino acid sequence alignment shows the level of conservation in diverse species of the amino acid Ala^{413} (red characters).

Figure 4. *In vitro* assay using HaCaT cells transfected with mutated *KRT14* cDNA

(a) Immunoblot analysis reveals that HaCaT cells transfected with either wild-type

(K14WT) or mutated *KRT14* cDNA (K14A413T and K14A413P) express V5-tagged K14 molecules. Equal protein loading was confirmed by reprobing with AC15 (anti-beta-actin antibody). (b-d) HaCaT cells transfected with K14WT (b) or K14A413T (c) or K14A413P (d) (bar: 5 μm). To visualize the transfected gene product, cells were stained with FITC-conjugated anti-V5 antibody. Cells transfected with K14WT and K14A413T have a normal keratin filament network (b, c), whereas significantly more cells transfected with K14A413P exhibit small ball-like clump formation (d). (e) The percentage of cells showing keratin aggregate formation among transfected cells is compared. There are significantly more clumps observed in the K14A413P-transfected cells (49±8%) than in those transfected with either K14WT (17±3%) or K14A413T (6±4%). Each value shown represents the mean ± SEM of ten individual samples. The statistical significance of the differences between groups is assessed by one-way ANOVA followed by Tukey's test (*, $p < 0.05$).

Supplementary figure legends

Supplementary Figure 1. *In vitro* assay using HaCaT cells cotransfected with K14A413P/K14A413T or K14A413P/K14WT

The percentage of cells showing keratin clumping among transfected HaCaT cells is compared. Each value shown represents the mean ± SEM of ten individual samples. There is no statistically significant difference in the percentage of clumped cells between K14A413P/K14A413T (32±5%) and K14A413P/K14WT (30±5%) (Student's t-test, $p > 0.05$). HaCaT cells transfected with K14A413P alone are used as control (the percentage of clumped cells; 42±6%).

Supplementary Figure 2. *In vitro* assay using HeLa cells transfected with mutated *KRT14* cDNA

The percentage of cells showing keratin aggregates among transfected HeLa cells is compared. Each value shown represents the mean ± SEM of ten individual samples. There are significantly more keratin clumped cells observed in the K14A413P-transfected HeLa cells (77±7%) than in those transfected with either K14WT (14±4%) or K14A413T (10±4%). The statistical significance of the differences between groups is assessed by one-way ANOVA followed by Tukey's test (*, $p < 0.05$).

Supplementary Figure 3. *In vitro* assay using normal human epidermal keratinocytes transfected with mutated *KRT14* cDNA

Normal human epidermal keratinocytes (NHEK) transfected with K14WT (a) or K14A413T (b) or K14A413P (c) (bar: 5 μm). No keratin aggregates were observed in any of the groups.

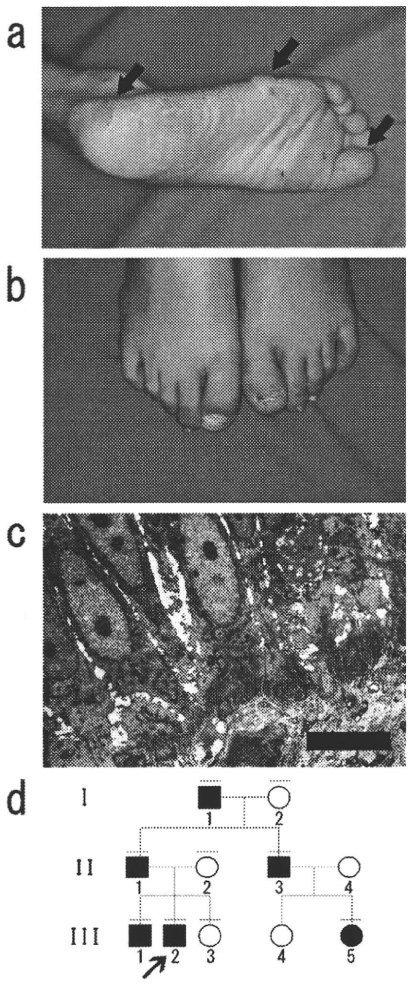

Figure 1. Clinical and ultrastructural features of a family with epidermolysis bullosa simplex
(a) Blisters and erosions are seen in the proband's right sole (arrows). (b) Toenail deformities are observed in the proband. (c) Ultrastructural features of the proband lesional skin sample show basal cell cytolysis (bar: 5 μm). No apparent keratin clumps are seen. (d) Pedigree of the proband's family. Affected individuals are indicated by black fill. The proband is indicated by an arrow.
117x299mm (300 x 300 DPI)

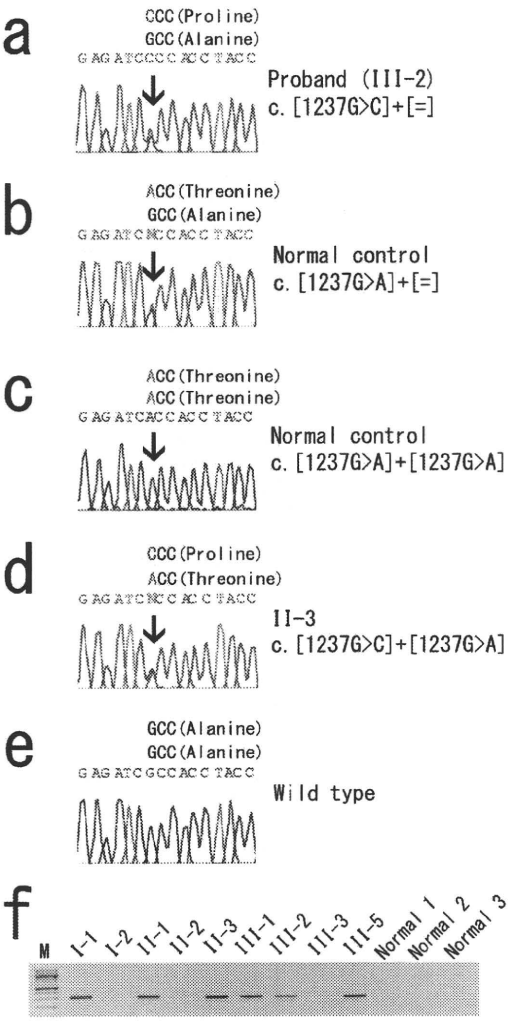

Figure 2. KRT14 mutation analysis
(a) The proband (III-2) is heterozygous for c.1237G>C (p.Ala413Pro) in KRT14 (an arrow). (b) 2 out of 100 normal controls are heterozygous for c.1237G>A (p.Ala413Thr) (an arrow). (c) 1 out of 100 normal controls is homozygous for c.1237G>A (p.Ala413Thr) (an arrow). (d) The proband's uncle (II-3) is compound heterozygous for c.1237G>C (p.Ala413Pro) and c.1237G>A (p.Ala413Thr) (an arrow). (e) The wild-type sequence. (f) Mutant-allele specific amplification shows that affected family members (Fig. 1d) harbor c.1237G>C (p.Ala413Pro).
199x399mm (300 x 300 DPI)

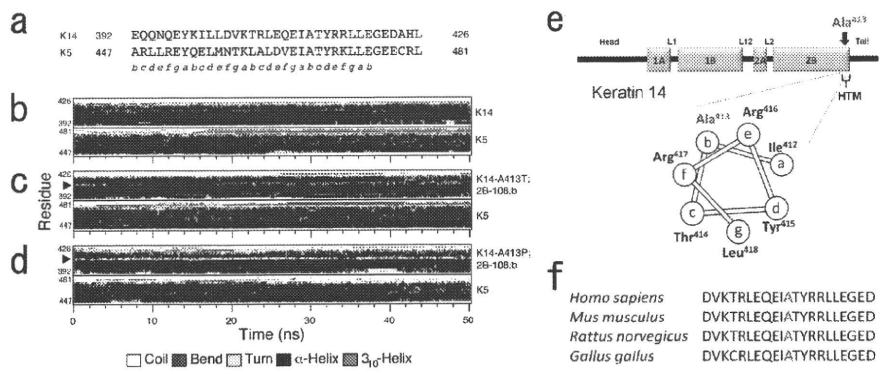

Figure 3. Molecular dynamics of the keratin heterodimer
(a) Sequences of the keratin helix motif and the heptad repeat positions in K5 and K14. (b-d) Molecular dynamics simulations. The changes in secondary structure due to an amino acid substitution were visualized through the molecular dynamics. These simulations were each run for 50.0 ns. Blue indicates the alpha-helix. The native (b) and p.Ala413Thr (c) peptides retain alpha-helix geometry (blue-colored) throughout the simulation. In contrast, increased instability in the alpha-helix was observed in the p.Ala413Pro mutant peptide (d) bound with K5, which is indicated by the appearance of yellow-colored turn motif (arrow heads). In the p.Ala413Pro peptide (d), the helical geometry at the C-terminus of both K14 and K5 is substantially compromised throughout the simulation - K5 is unstructured (coil geometry), and K14 alternates between coil, bend and turn geometries. (e) A schematic diagram of K14 structure. Note that Ala413 is located at the helix termination motif (HTM) of the keratin molecule. Ala413 corresponds to position 'b' of the heptad repeat (abcdefg), and is conserved among keratin polypeptides. (f) K14 amino acid sequence alignment shows the level of conservation in diverse species of the amino acid Ala413 (red characters).
399x199mm (300 x 300 DPI)

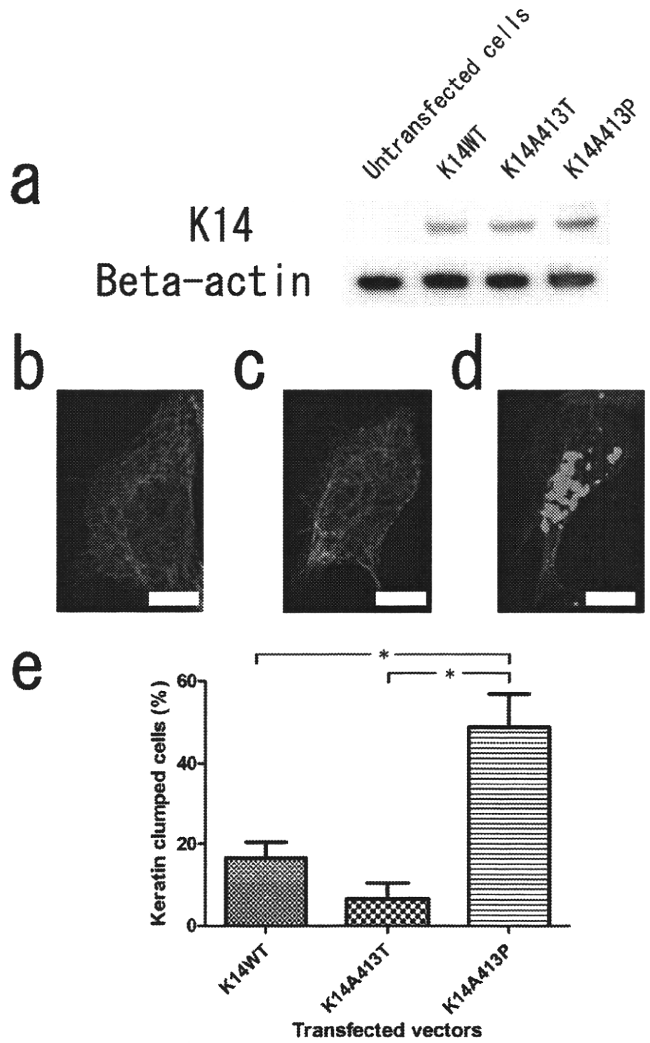

Figure 4. In vitro assay using HaCaT cells transfected with mutated KRT14 cDNA
(a) Immunoblot analysis reveals that HaCaT cells transfected with either wild-type (K14WT) or mutated KRT14 cDNA (K14A413T and K14A413P) express V5-tagged K14 molecules. Equal protein loading was confirmed by reprobing with AC15 (anti-beta-actin antibody). (b-d) HaCaT cells transfected with K14WT (b) or K14A413T (c) or K14A413P (d) (bar: 5 μm). To visualize the transfected gene product, cells were stained with FITC-conjugated anti-V5 antibody. Cells transfected with K14WT and K14A413T have a normal keratin filament network (b, c), whereas significantly more cells transfected with K14A413P exhibit small ball-like clump formation (d). (e) The percentage of cells showing keratin aggregate formation among transfected cells is compared. There are significantly more clumps observed in the K14A413P-transfected cells (49±8%) than in those transfected with either K14WT (17±3%) or K14A413T (6±4%). Each value shown represents the mean ± SEM of ten individual samples. The statistical significance of the differences between groups is assessed by one-way ANOVA followed by Tukey's test (*, $p < 0.05$).

99x156mm (300 x 300 DPI)

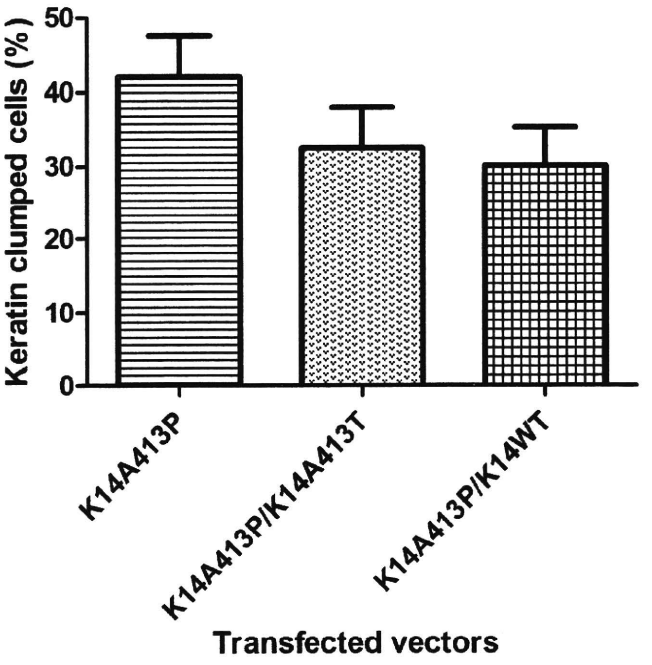

Supplementary Figure 1. *In vitro* assay using HaCaT cells cotransfected with K14A413P/K14A413T or K14A413P/K14WT

The percentage of cells showing keratin clumping among transfected HaCaT cells is compared. Each value shown represents the mean ± SEM of ten individual samples. There is no statistically significant difference in the percentage of clumped cells between K14A413P/K14A413T (32±5%) and K14A413P/K14WT (30±5%) (Student's t-test, $p > 0.05$). HaCaT cells transfected with K14A413P alone are used as control (the percentage of clumped cells; 42±6%).